IEEE Access
Multidisciplinary | Rapid Review | Open Access Journal

Date of publication xxxx 00, 0000, date of current version xxxx 00, 0000.

Digital Object Identifier 10.1109/ACCESS.2017.Doi Number

Robust Backstepping Super-Twisting Sliding Mode Control for Autonomous Vehicle Path Following

Di Ao[1], Wei Huang[2, 3], Pak Kin Wong[1], and Jialin Li[4]

[1]Department of Electromechanical Engineering, University of Macau, Macau SAR 999078, China
[2]School of Mechanical Engineering and Automation, Fuzhou University, Fuzhou 350108, China
[3]Xiamen Golden Dragon Bus Company Ltd., Xiamen 361028, China
[4]School of Electromechanical Engineering, Guangdong University of Technology, Guangzhou 510006, China

Corresponding authors: Wei Huang and Pak Kin Wong (e-mail: huangweiamoy@gmail.com; fstpkw@um.edu.mo).

This work was supported in part by the University of Macau under Grant No. MYRG-2019-00028-FST and MYRG2020-00045-FST, and in part by the Youth Teacher Educational Research Fund of the Fujian Provincial Education Office under Grant No. JAT200013, and in part by the Natural Science Foundation of Guangdong Province of China under Grant No. 2019A1515011602.

ABSTRACT This paper focuses on the path following control problems for autonomous driving vehicles. Aiming at enhancing the robustness and attenuating the chattering phenomenon, a super-twisting sliding mode control algorithm (STA) is developed based on Lyapunov theory, where the proof of the stability of the control system is presented by applying the backstepping technique. Moreover, co-simulation between Matlab/Simulink and Carsim is carried out to verify the path following control performance. In this research, *Stanley* controller, conventional sliding mode control (SMC), and model predictive control (MPC) are used as the benchmark controllers for evaluating the proposed STA performance. Two driving scenarios are considered in the simulations, including normal driving and fierce driving. To comprehensively assess the control performance and control effort (i.e. magnitude of steering), an integrated and weighted performance evaluation index ($IWPEI$) is novelly provided. Simulation results show that the $IWPEI$ of the proposed STA can be reduced by 40.5%, 25.8%, 10.9% in the normal driving scenario; and 62.5%, 24%, 6.8% in the fierce driving scenario as compared with *Stanley* controller, conventional SMC, and MPC, respectively. The results also indicate that the proposed STA outperforms the conventional SMC in terms of the chattering attenuation, resulting in a smoother front steering wheel angle input and a smoother yaw rate performance. As compared with MPC, the advantage of the proposed STA lies in its much lower computational complexity. Furthermore, the robustness of the controllers is verified by changing the vehicle mass and tire parameters. The proposed STA can reduce the fluctuation of the $IWPEI$ by 22.6%, 22.3%, and 5.9% compared with the benchmark approaches. These results imply that the consideration of system perturbations is very critical in the design of the super-twisting sliding mode controller which can improve the robustness of the autonomous vehicle path following system.

INDEX TERMS Path following control, super-twisting sliding mode, backstepping, robustness, perturbations.

I. INTRODUCTION

Autonomous vehicles receive more and more attention nowadays with the ever-increasing safety transportation requirements. The famous "*DAPRA Grand Challenge*" and "*DAPRA Urban Challenge*" began in the U.S. more than ten years ago [1] to foster the development of autonomous driving (AD) technology. It is well known that AD is a hard and complex technology for putting it into practical use and mass production, especially for the trajectory tracking problems under high velocity [2]. It demands the steering system automatically steers the vehicle to follow the desired path. Besides, it should also maintain driving safety, lateral stability, and comfort simultaneously [3]. However, the path following control is very challenging due to high system nonlinearity, perturbations, and influence on other vehicle performances [4-9].

The goal of the trajectory tracking control is to minimize the lateral deviation as much as possible and maintain an acceptable yaw rate simultaneously [10, 11]. The existing researches generally adopt three types of vehicle models for the path following controller design, including geometric-based model, kinematic-based model, and dynamic model. The three different models describe the geometrical configuration of the steering system (mainly the Ackerman steering system), the kinematic relationship of the vehicle motion, and the vehicle dynamic motion with internal states, respectively [5]. As reported, many vehicles in the *DAPRA* competition use the geometric-based model to design the steering controller. Meanwhile, many researchers use the kinematic model for controller development [1, 12]. However, due to the negligence of the internal dynamics of the model, the geometric and kinematic-based controllers have some limitations for practical applications [13]. Therefore, the dynamic vehicle model-based controllers are mostly used in trajectory following controller design recently [10, 11, 14-18].

Linear, nonlinear, and optimization control methods were employed by many studies on model-based controllers for trajectory following [3, 19-31]. The famous *Stanley* steering control law was designed based on the non-linear feedback function of lateral deviation, and exponential convergence is obtained under some assumptions in [1]. However, it is unsuitable for passenger vehicles as it is mainly designed for lower longitudinal vehicle speed. In [32], a robust H_∞ controller based on a linear parameter varying (LPV) model is developed to improve the path tracking performance. The internal parameter uncertainties are incorporated into the polytopic model, which consists of eight sub-models. However, the external disturbances are not discussed. In [33, 34], the authors developed and compared three types of trajectory tracking controllers, namely, super twisting sliding mode controller (ST-SMC), immersion and invariance controller (I&I), and adaptive passivity-based controller (APBC). These controllers were regarded as nonlinear proportional and integral control methods. The control performances were verified through a driver simulator SCANeR Studio, and the results showed all three controllers had good tracking performance. However, the external disturbances and internal parameter variations (e.g. vehicle mass variation, change of cornering stiffness, etc.) are not sufficiently considered during the controller design. Hence, the I&I controller is sensitive to the parameter uncertainties and the APBC has a high possibility to request high control gains during a large curvature variation. The high gains are prone to cause more energy consumption and input saturation. For the ST-SMC controller in [33], it combines a square-root correction term and the integral of the high gain switch function to the steering input angle. Even though the control law is the simplest one among the three controllers, the proposed ST-SMC is sensitive to disturbances or parametric uncertainties, resulting in significant peaks during the rapid variation of curvature. Another form of SMC entitled integral sliding mode (ISM) was proposed in [4] to improve the chattering phenomenon and control performance. The ISM is combined with composite nonlinear feedback (CNF) controller for controlling the front wheel steering angle to track the desired path, which has smaller overshoots and lateral deviation as compared with the pure CNF controller [35]. However, the longitudinal speed variation and the unmodeled dynamics (i.e. perturbations) are not covered in this research. Besides, linear and nonlinear model predictive control (MPC) was used in [36, 37] to design the path following controller. In [36], the changing road conditions and the small-angle simplification for the vehicle sideslip angle are cast into a measurable disturbance. The discrete previewed path points are used to construct the objective function to improve the performance under lower acceleration in [37]. To improve the computational efficiency in addressing the non-linear optimization problem, [38] adopted a continuous-time finite-horizon approximate dynamic programming method. Nevertheless, the relatively heavy computation burden is still the major problem with using the MPC for practical vehicles.

For the evaluation of path-following control performance, most of the researches [7,8,12,13] only took the mean absolute error (MAE) of lateral deviation and heading angle with respect to the desired trajectory. Honestly, the evaluation indexes are probably not fair because the control effort and the product of error and time are not taken into account. These factors are pretty critical to objectively assess the control performance. Hence, it is recommended to propose a novel integrated and weighted index for a comprehensive evaluation of the controller.

To this end, this paper aims to develop a path following controller which can overcome the chattering problem of the front steering angle input with good robustness in response to external or internal perturbations under the premise of taking less control effort and computation time. Based on these requirements, a novel super-twisting sliding mode control method with consideration of perturbations is developed in this work. The contributions of this study are summarized as follows: 1) A novel super-twisting sliding mode control algorithm (STA) considering the external and internal perturbations is proposed for path following. Due to the consideration of the perturbations, the proposed super-twisting sliding mode controller can improve the accuracy and robustness in the path following problem for autonomous vehicles; 2) The stability of the proposed controllers is proved using the Lyapunov method, in which the backstepping technique is applied to simplify the proof of the controller stability; 3) A novel integrated and weighted performance evaluation index ($IWPEI$) is proposed to more fairly assess the control performance under the same conditions.

The remainder of this paper is organized as follows. Section II describes vehicle dynamic modeling, control problem formulation, and steering system constraints. *Stanley* controller, conventional SMC, MPC, and the proposed STA controllers are presented in Section III. The simulation results

This article has been accepted for publication in a future issue of this journal, but has not been fully edited. Content may change prior to final publication. Citation information: DOI 10.1109/ACCESS.2021.3110435, IEEE Access

and discussion are shown in Section IV. Finally, Section V gives a conclusion.

II. AUTONOMOUS GROUND VEHICLE MODELING AND CONTROL PROBLEM FORMULATION

The path following control for an autonomous vehicle is requested to track the reference path as accurately as possible. It is assumed that the longitudinal speed is changed slowly $\dot{V}_x = 0$. The planar motion is mainly considered during the path following process. The following parts concern the vehicle dynamic model and control problem formulation.

A. SINGLE-TRACK MODEL

A schematic diagram for a single-track vehicle model is shown in Figure 1. Generally, the front steering angle is assumed to be a small angle [37]. The planar motion of the autonomous vehicle can be formulated to represent the lateral dynamic behavior (sideslip angle β, yaw rate $\dot{\varphi}$). The side slip angles of tires on the same axle are assumed as the same. The roll and pitch dynamics are neglected for simplification. The front steering wheel angle δ_f and sideslip angle β are considered as small angles under normal driving conditions. Then a linear tire lateral force region can be obtained. Based on these assumptions, a linear parameter varying (LPV) model can be constructed, where the longitudinal velocity V_x is regarded as a varying parameter [39]. The dynamic single-track model in terms of sideslip angle and yaw rate $\dot{\varphi}$ is shown as below:

$$\begin{cases} \dot{\beta} = -\dfrac{\mu(C_f + C_r)}{mV_x}\beta - \left(1 + \dfrac{\mu(l_f C_f - l_r C_r)}{mV_x^2}\right)\dot{\varphi} \\ \qquad + \dfrac{\mu C_f}{mV_x}\delta_f \\ \ddot{\varphi} = -\dfrac{\mu(l_f C_f - l_r C_r)}{I_z}\beta - \dfrac{\mu(l_f^2 C_f + l_r^2 C_r)}{I_z V_x}\dot{\varphi} \\ \qquad + \dfrac{\mu l_f C_f}{I_z}\delta_f . \end{cases} , \quad (1)$$

where μ is the road friction coefficient, m is the vehicle mass, l_f and l_r are the distances of Center of Gravity (CG) to front axle and rear axle, I_z is the yaw moment of inertia, C_f and C_r are cornering stiffness of front and rear tires. Here the cornering stiffness is considered twice over a single tire [40]. The following part introduces the control problem formulation.

B. CONTROL PROBLEM FORMULATION

As shown in Figure 2, the path following problem can be considered as minimizing the lateral deviation of the automatic pilot vehicle with respect to the predefined reference path. The second-order deviation of the lateral error is denoted as

$$\ddot{e} = a_y - a_{ref} , \quad (2)$$

where a_y represents the actual lateral acceleration of the vehicle; a_{ref} denotes the desired lateral acceleration on the designed path.

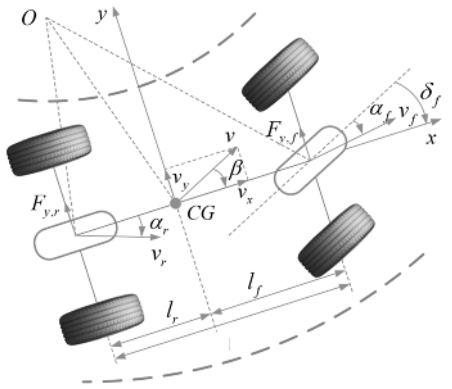

FIGURE. 1. Single-track vehicle model for planar motion.

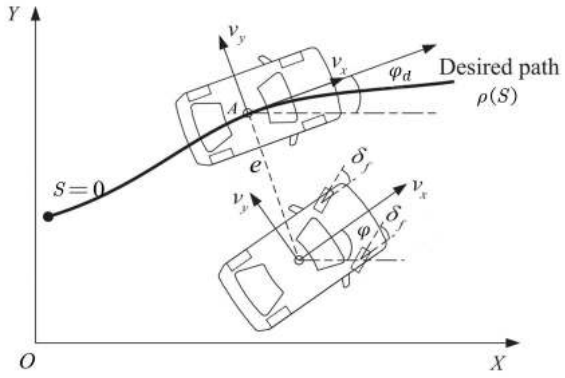

FIGURE. 2. Lateral deviation from vehicle to the desired path.

The reference lateral acceleration can be written as

$$a_{ref} = \rho(S)V_x^2 , \quad (3)$$

where $\rho(S)$ is the curvature of the reference path, and S is the displacement. Assume the actual lateral acceleration is given by $a_y = V_x(\dot{\beta} + \dot{\varphi})$, then

$$\ddot{e} = V_x(\dot{\beta} + \dot{\varphi}) - \rho(S)V_x^2 . \quad (4)$$

Substituting (1) into (4), the following error dynamics can be obtained:

$$\ddot{e} = -\frac{\mu(C_f + C_r)}{m}\beta - \frac{\mu(l_f C_f - l_r C_r)}{mV_x}\dot{\varphi} - \rho(S)V_x^2 + \frac{\mu C_f}{m}\delta_f . \quad (5)$$

By defining the state vector as $x = (\beta, \dot{\varphi}, \dot{e}, e)^{\mathrm{T}}$, which corresponds to vehicle sideslip angle, yaw rate, the first derivative of lateral error, and lateral error, the control input as front steering angle δ_f, the reference curvature $\rho(S)$ as external disturbance, the following system equation can be obtained:

$$\dot{x} = Ax + B_1 u + B_2 d , \quad (6)$$

where

This article has been accepted for publication in a future issue of this journal, but has not been fully edited. Content may change prior to final publication. Citation information: DOI 10.1109/ACCESS.2021.3110435, IEEE Access

$$A=\begin{bmatrix} -\frac{\mu(C_f+C_r)}{mV_x} & -1-\frac{\mu(l_fC_f-l_rC_r)}{mV_x^2} & 0 & 0 \\ -\frac{\mu(l_fC_f-l_rC_r)}{I_z} & -\frac{\mu(l_f^2C_f+l_r^2C_r)}{I_zV_x} & 0 & 0 \\ -\frac{\mu(C_f+C_r)}{m} & -\frac{\mu(l_fC_f-l_rC_r)}{mV_x} & 0 & 0 \\ 0 & 0 & 1 & 0 \end{bmatrix},$$

$$B_1=\begin{bmatrix} \frac{\mu C_f}{mV_x} \\ \frac{\mu l_f C_f}{I_z} \\ \frac{\mu C_f}{m} \\ 0 \end{bmatrix}, B_2=\begin{bmatrix} 0 \\ 0 \\ -V_x^2 \\ 0 \end{bmatrix}, u=\delta_f, d=\rho(S).$$

Under the predefined curvature and longitudinal velocity for the desired trajectory, the desired control target is $\dot{e}=e=0$.

The desired sideslip angle and yaw rate for a linear vehicle model is

$$\begin{cases} \beta_{ref}=\left(l_r-\frac{l_fmV_x^2}{\mu C_r(l_f+l_r)}\right)\rho(S) \\ \dot{\varphi}_{ref}=V_x\rho(S). \end{cases} \quad (7)$$

The desired equilibrium point of the state is given by $x_{eq}=(\beta,\dot{\varphi},\dot{e},e)^{\mathrm{T}}=(\beta_{ref},\dot{\varphi}_{ref},0,0)^{\mathrm{T}}$. The control input at the equilibrium point is obtained as follows:

$$\delta_{ref}=(l_f+l_r)\rho(S)+\frac{mV_x^2(l_rC_r-l_fC_f)}{\mu C_fC_r(l_f+l_r)}\rho(S). \quad (8)$$

The sideslip angle error, yaw rate error, and front steering angle are derived as

$$\begin{cases} \tilde{\beta}=\beta-\beta_{ref} \\ \dot{\tilde{\varphi}}=\dot{\varphi}-\dot{\varphi}_{ref} \\ \tilde{\delta}=\delta_f-\delta_{ref} \end{cases}. \quad (9)$$

As previously mentioned, the steady-state solution to the single-track model can be found in (7) and (8). Substituting (9) into the control system represented in (6), the following system is generated as

$$\dot{\tilde{X}}=A\tilde{X}+B_1\tilde{\delta}_f. \quad (10)$$

The new equilibrium point becomes $\dot{X}_{eq}=(\tilde{\beta},\dot{\tilde{\varphi}},\dot{e},e)^{\mathrm{T}}=(0,0,0,0)^{\mathrm{T}}$. The target system of Model (9) under $\dot{e}=e=0$ can be expressed as

$$\begin{cases} \dot{\tilde{\beta}}=-\dot{\tilde{\varphi}} \\ \ddot{\tilde{\varphi}}=\frac{\mu C_r(l_f+l_r)}{I_z}\tilde{\beta}-\frac{\mu l_rC_r(l_f+l_r)}{I_zV_x}\dot{\tilde{\varphi}} \end{cases}. \quad (11)$$

It is easily verified that the equilibrium origin of System (10) is at the $(0,0)$. Let $\Xi=[\tilde{\beta}\quad\dot{\tilde{\varphi}}]^{\mathrm{T}}$, then (11) can be rewritten as $\dot{\Xi}=\Theta\Xi$ with

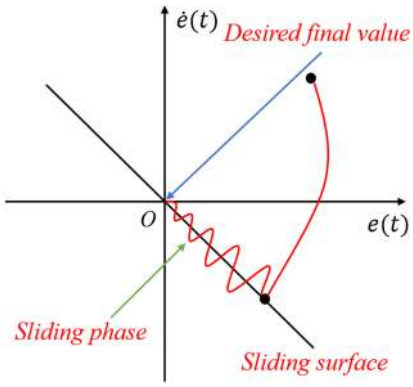

FIGURE. 3. Graphical interpretation of sliding mode control.

$$\Theta=\begin{bmatrix} 0 & -1 \\ \frac{\mu C_r(l_f+l_r)}{I_z} & -\frac{\mu l_rC_r(l_f+l_r)}{I_zV_x} \end{bmatrix}. \quad (12)$$

By taking the Laplace transformation, the characteristic polynomial is obtained as

$$\det(s_LI-\Theta)=s_L^2+\frac{\mu l_rC_r(l_f+l_r)}{I_zV_x}s_L+\frac{\mu C_r(l_f+l_r)}{I_z}, \quad (13)$$

where s_L is the Laplace operator. In (13), the following parameters (C_r,l_f,l_r,I_z,V_x) are all considered as positive values. Then, Matrix Θ can meet the Routh–Hurwitz stability conditions with longitudinal velocity large than zero, which means the global equilibrium origin of System (10) is $(0,0)$.

C. STEERING SYSTEM CONSTRAINTS

The controller designed in this research directly controls the front steering wheel angle. Hence, a set of constraints on the magnitudes of steering and the rate of steering are considered to achieve a smooth transition. The following inequalities are used to saturate the steering system output:

$$\begin{aligned} -20\mathrm{deg}\le\delta_f\le 20\mathrm{deg} \\ -25\mathrm{deg/s}\le\dot{\delta}_f\le 25\mathrm{deg/s}. \end{aligned} \quad (14)$$

III. PATH FOLLOWING CONTROLLER DESIGN

The variable structure sliding control method has been widely used due to its high robustness with respect to model uncertainty and disturbance. The control objective is to force the system states eventually to stay on a pre-designed sliding surface. Figure 3 is a phase-plane graphical representation for sliding mode control, which shows the control objective for tracking error and its derivative. The state path can converge and stay along the pre-designed sliding surface. In this section, a standard *Stanley* controller and a non-linear MPC in the existing research are introduced as the

This article has been accepted for publication in a future issue of this journal, but has not been fully edited. Content may change prior to final publication. Citation information: DOI 10.1109/ACCESS.2021.3110435, IEEE Access

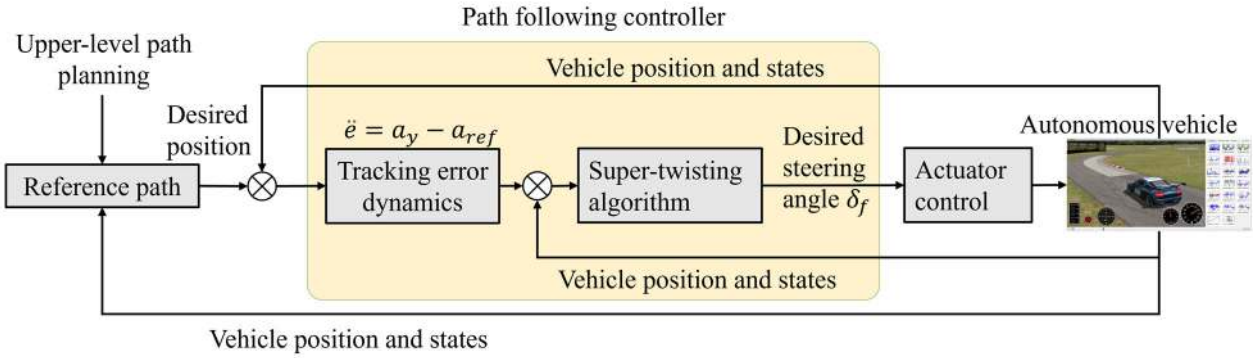

FIGURE. 4. Structure of proposed path following controller.

benchmark controllers for comparison. Besides, a conventional SMC controller is developed without considering the perturbations, whereas a novel STA controller is designed by considering the system perturbations. As the benchmark, the non-linear MPC controller used for trajectory tracking refers to [37]. The details for controller design steps are shown in the following subsections. The proposed STA controller structure is depicted in Figure 4. It receives upper-level path information as well as the vehicle position and states. Based on the formulated tracking error dynamics, the desired steering angle can be computed accordingly.

A. BENCHMARK Ⅰ - STANLEY CONTROLLER

Stanley controller is firstly proposed in [1] by Stanford University for *DARPA* Challenge. The steering angle is denoted as below:

$$\delta_f = e_\varphi + \arctan\left(\frac{ke}{V_x}\right), \tag{15}$$

where e_φ denotes the heading error with respect to an ideal trajectory. It can be calculated according to the Serret-Frenet frame. k represents the positive controller gain which determines the decay rate. The stability proof is omitted here for simplification, but it can be found in [1]. For this research, the *Stanley* controller is introduced as a benchmark controller for comparison.

B. BENCHMARK Ⅱ - CONVENTIONAL SMC

This subsection shows a conventional SMC controller from existing literature. The lateral deviation concerning a reference is minimized by adopting the algorithm. The details refer to [33, 34].

A general form for the sliding surface is designed as

$$s = \dot{e} + \lambda e\,, \tag{16}$$

where λ is a positive real number. By taking the derivative of (16), the following equation can be obtained:

$$\dot{s} = \ddot{e} + \lambda \dot{e}\,. \tag{17}$$

Substituting (5) into (17), the first derivative of the sliding surface is expressed as

$$\dot{s} = -\frac{\mu(C_f + C_r)}{m}\beta - \frac{\mu(l_f C_f - l_r C_r)}{mV_x}\dot{\varphi} - \rho(S)V_x^2 + \frac{\mu C_f}{m}\delta_f + \lambda\dot{e}\,. \tag{18}$$

The relative degree between the sliding surface and control input equals one, as illustrated by (18). Then the control law can be derived in a general rule. It is known that the common structure of SMC control input consists of an equivalent command δ_{EQ} and a switching function δ_{SW} of a discontinuous signal. The equivalent command δ_{EQ} acts as an auxiliary control command added to the control input. δ_{EQ} is derived from the equation $\dot{s} = 0$. The equivalent command aims to drive the system to the sliding surface. It is given by

$$\begin{cases} \delta_{EQ} = \dfrac{C_f + C_r}{C_f}\beta + \dfrac{l_f C_f - l_r C_r}{C_f V_x}\dot{\varphi} + \dfrac{mV_x^2}{\mu C_f}\rho(S) - \dfrac{m\lambda}{\mu C_f}\dot{e} \\ \delta_{SW} = -\dfrac{m\alpha_1}{\mu C_f}\mathrm{sign}(s) \end{cases}, \tag{19}$$

where α_1 is a positive coefficient. Generally, a big value is assigned to α_1 for the finite-time convergence and robustness improvement.

Proposition 1: If the total control input is defined as the sum of equivalent and switching functions:

$$\delta_f = \delta_{SW} + \delta_{EQ}\,, \tag{20}$$

the conventional SMC controller performs the finite-time convergence and the proof of controller stability is followed by Lyapunov theory.

Proof: A Lyapunov candidate is designed as

$$V_0(t) = \frac{1}{2}s^2. \tag{21}$$

The first derivative of the Lyapunov function is obtained as

$$\begin{aligned}\dot{V}_0(t) &= s\cdot\dot{s}\\ &= s\cdot\left(-\frac{\mu(C_f+C_r)}{m}\beta-\frac{\mu(l_fC_f-l_rC_r)}{mV_x}\dot{\varphi}-\right.\\ &\left.\rho(S)V_x^2+\frac{\mu C_f}{m}\delta_f+\lambda\dot{e}\right).\end{aligned} \tag{22}$$

Substituting (19) and (20) into (22), the following expression can be formulated:

$$\begin{aligned}\dot{V}_0(t) &= s\cdot\dot{s}\\ &= s\cdot\left[-\frac{\mu(C_f+C_r)}{m}\beta-\frac{\mu(l_fC_f-l_rC_r)}{mV_x}\dot{\varphi}-\right.\\ &\rho(S)V_x^2+\frac{\mu C_f}{m}\left(\frac{C_f+C_r}{C_f}\beta+\frac{l_fC_f-l_rC_r}{C_fV_x}\dot{\varphi}+\right.\\ &\left.\left.\frac{mV_x^2}{\mu C_f}\rho(S)-\frac{m\lambda}{\mu C_f}\dot{e}-\frac{m\alpha_1}{\mu C_f}\mathrm{sign}(s)\right)+\lambda\dot{e}\right]\\ &= s\cdot\left(-\alpha_1\mathrm{sign}(s)\right)\\ &= -\alpha_1|s|\le 0\,.\end{aligned} \tag{23}$$

On the basis of the above analysis, it is seen that the conventional SMC controller will converge to zero in a limited time. Indeed, the conventional SMC control law drives the state trajectories of the control system to a pre-designed sliding surface by using the inconsecutive signum function. The next part of this section presents the design of the proposed STA by considering the perturbations.

C. SUPER-TWISTING ALGORITHM WITH PERTURBATIONS

This part develops an STA control law considering the unmodelled dynamics and disturbances. The error dynamics is given by

$$\begin{aligned}\ddot{e} = &-\frac{\mu\left(C_f+C_r\right)}{m}\beta-\frac{\mu\left(l_fC_f-l_rC_r\right)}{mV_x}\dot{\varphi}\\ &-\rho(S)V_x^2+\frac{\mu C_f}{m}\delta_f+\xi(t)\,,\end{aligned} \tag{24}$$

where $\xi(t)$ is considered as the perturbations containing the external disturbance and unmodeled dynamics. Here a new state vector $z=[z_1 \quad z_2]^T$ is introduced with $z_1=e$, and $z_2=\dot{e}$. Rewriting (24) as a state-space function, the following equation is obtained:

$$\begin{cases}\dot{z}_1=z_2\\ \dot{z}_2=-\dfrac{\mu\left(C_f+C_r\right)}{mV_x}\beta-\dfrac{\mu\left(l_fC_f-l_rC_r\right)}{mV_x^2}\dot{\varphi}.\\ \qquad -\rho(S)V_x^2+\dfrac{\mu C_f}{m}\delta_f+\xi(t,z)\end{cases} \tag{25}$$

Assuming that the two desired tracking references are given as z_{1d} and z_{2d}, respectively. In this research, the desired state values are set to zero. The corresponding errors are given as below:

$$\begin{cases}e=z_1-z_{1d}\\ \dot{e}=z_2-z_{2d}\end{cases}. \tag{26}$$

Proposition 2: If the control input is designed as (27), which yields the finite-time convergence of the designed sliding surface to zero. The introduced new states $z_1$and z_2 converge to zero in finite time.

$$\begin{cases}\delta_f=\dfrac{C_f+C_r}{C_f}\beta+\dfrac{l_fC_f-l_rC_r}{C_fV_x}\dot{\varphi}+\dfrac{mV_x^2}{\mu C_f}\rho(S)\\ \quad-\dfrac{m\lambda}{\mu C_f}\dot{e}-\dfrac{k_1m|s|^{\frac{1}{2}}\mathrm{sign}(s)}{C_f}-\dfrac{k_2m}{C_f}\displaystyle\int_0^t\mathrm{sign}(s)dt\\ k_1>\dfrac{(\lambda_1+\lambda_2^2-2\xi^+)^2-8\lambda_2^2\xi^+}{4\lambda_1\lambda_2}>0,k_2=\dfrac{1}{2}\lambda_2k_1\\ \lambda_1>0\\ \lambda_2\in R\end{cases}, \tag{27}$$

where $\xi^+>0$ is considered as the upper bound of $\dot{\xi}(t,z)$, and hence $\left|\dot{\xi}(t,z)\right|\le\xi^+$. The details for proof are shown below.

Proof: To prove the closed-loop stability of the controller, the first derivative of the sliding surface is given as

$$\dot{s}=(\dot{z}_2-\ddot{z}_{1d})+\lambda\dot{e}. \tag{28}$$

Substituting the predesigned control law (27) and (25) into (28), the following equation can be generated:

$$\begin{aligned}\dot{s} = &-k_1m|s|^{\frac{1}{2}}\mathrm{sign}(s)-k_2\int_0^t\mathrm{sign}(s)dt\\ &+\xi(t,z).\end{aligned} \tag{29}$$

Equation (29) also shows the dynamic requirement of the sliding surface. To simplify the proof of stability, the backstepping technique is used. The new variables η_1 and η_2 are put forward accordingly. A new tuple $[\eta_1 \quad \eta_2]$ is introduced to rewrite (29) for further simplification suggested by [41, 42]:

$$\begin{cases}\eta_1=s\\ \eta_2=-k_2\displaystyle\int_0^t\mathrm{sign}(s)dt+\xi(t,z)\end{cases}. \tag{30}$$

By taking the first derivatives of η_1 and η_2, and rearranging the terms, the sliding surface differential inclusion is given as

$$\begin{cases}\dot{\eta}_1=-k_1|\eta_1|^{\frac{1}{2}}\mathrm{sign}(\eta_1)+\eta_2\\ \dot{\eta}_2=-k_2\mathrm{sign}(\eta_1)+\dot{\xi}(t,z)\end{cases}. \tag{31}$$

Equation (31) can be reformulated as a new state-space model by introducing a new state vector $\varrho=[\varrho_1 \quad \varrho_2]^T=\left[|\eta_1|^{\frac{1}{2}}\mathrm{sign}(\eta_1) \quad \eta_2\right]^T$. Then, (31) can be written in terms of ϱ_1 and ϱ_2,

$$\begin{cases}\dot{\varrho}_1=\dfrac{1}{2|\varrho_1|}(-k_1\varrho_1+\varrho_2)\\ \dot{\varrho}_2=\dfrac{1}{2|\varrho_1|}(-2k_1\varrho_1)+\dot{\xi}(t,z)\end{cases}. \tag{32}$$

As aforementioned, $\dot{\xi}(t,z)$ is a bounded signal, then it can be expressed as

$$\dot{\xi}(t,z)=\sigma(t,z)\mathrm{sign}(\eta_1)=\sigma(t,z)\frac{\varrho_1}{|\varrho_1|}, \tag{33}$$

where $\sigma(t,z)$ is a bounded function satisfying $0 < \sigma(t,z) < \xi^+$. Equation (32) can be rewritten as

$$\begin{bmatrix}\dot{\varrho}_1\\ \dot{\varrho}_2\end{bmatrix} = \underbrace{\frac{1}{2|\varrho_1|}\begin{bmatrix}-k_1 & 1\\ -2k_2+2\sigma & 0\end{bmatrix}}_{F(\varrho_1)}\begin{bmatrix}\varrho_1\\ \varrho_2\end{bmatrix}. \tag{34}$$

Remark: If the new state vector $\varrho = [\varrho_1 \quad \varrho_2]^T$ converges to zero within a limited time, η_1 and η_2 converge to zero within a limited time.

Proof: The Lyapunov candidate function for the proof of the convergence of ϱ_1 and ϱ_2 is selected as

$$V_1(\varrho) = \varrho^T P \varrho\,, \tag{35}$$

where the symmetric matrix P is defined as

$$P = P^T = \begin{bmatrix}\lambda_1+\lambda_2^2 & -\lambda_2\\ -\lambda_2 & 1\end{bmatrix}. \tag{36}$$

In (36), P is a positive definite matrix since $\lambda_1 > 0$ and λ_2 is an arbitrary real number. Therefore, the Lyapunov candidate function $V_1(\varrho)$ is a positive definite function. Taking the first derivative of the Lyapunov candidate function, the following equation is obtained:

$$\dot{V}_1(\varrho) = \varrho^T[PA(\varrho_1) + A^T(\varrho_1)P]\varrho. \tag{37}$$

Considering the upper bound of $\dot{\xi}(t,z)$, (37) can be rewritten as

$$\dot{V}_1(\varrho) \le -\frac{1}{2|\varrho_1|}\varrho^T Q \varrho. \tag{38}$$

where $Q = Q^T$; and Q is expressed as

$$Q = \begin{bmatrix}2\lambda_1 + 2\lambda_2^2 k_1 - 4\lambda_2 k_2 + 4\lambda_2\xi^+ & *\\ 2k_2 - \lambda_2 k_1 - \lambda_1 - \lambda_2^2 - 2\xi^+ & 2\lambda_2\end{bmatrix}. \tag{39}$$

where $*$ is the symmetric expression of a matrix.

By setting the gain $k_2 = 0.5\lambda_2 k_1$, (39) can be expressed as

$$Q = \begin{bmatrix}2\lambda_1 k_1 + 4\lambda_2\xi^+ & *\\ -(\lambda_1 + \lambda_2^2 + 2\xi^+) & 2\lambda_2\end{bmatrix}. \tag{40}$$

To make $\dot{V}_1(\varrho)$ as a semi-definite function, the matrix Q should be positive definite. Therefore, the controller gain k_1 is chosen as

$$k_1 > \frac{(\lambda_1 + \lambda_2^2 - 2\xi^+)^2 - 8\lambda_2^2\xi^+}{4\lambda_1\lambda_2}. \tag{41}$$

As the matrix P is dependent on the values of λ_1 and λ_2 (both of them are real numbers), the following inequality holds:

$$\begin{cases}\lambda_{min}\{P\}\|\varrho\|_2^2 \le V_1(\varrho) \le \lambda_{max}\{P\}\|\varrho\|_2^2\\ |\varrho_1| \le \|\varrho\|_2^2 \le \frac{V_1^{0.5}(\varrho)}{\lambda_{min}^{0.5}}\{P\}\end{cases}. \tag{42}$$

The derivative of the Lyapunov candidate function (35) can be rewritten as

$$\begin{aligned}\dot{V}_1(\varrho) &\le -\frac{1}{2|\varrho_1|}\lambda_{min}\{Q\}\|\varrho\|_2^2\\ &\le -\frac{1}{2|\varrho_1|}\lambda_{min}\{Q\}\frac{V_1(\varrho)}{\lambda_{max}\{P\}},\end{aligned} \tag{43}$$

where $\|\varrho\|^2 = |\varrho_1| + \varrho_2^2$, which means the two-norm of ϱ. By replacing (38) with (43), the following equation can be derived as

$$\begin{cases}\dot{V}_1(\varrho) \le -\varepsilon V^{0.5}(\varrho)\\ \text{with } \varepsilon = \dfrac{\lambda_{min}^{0.5}\{P\}\lambda_{min}\{Q\}}{2\lambda_{max}\{P\}}.\end{cases} \tag{44}$$

Since the solution of the equation is $\dot{v} = -\varepsilon v^{0.5}$ and $v(0) = v_0 \ge 0$, $v(t)$ is given as

$$v(t) = (v_0^{0.5} - 0.5\varepsilon t)^2\,, \tag{45}$$

where t denotes the time. It conforms to the comparison principle in [43] that $V_1(\varrho) \le v(t)$ when $V_1(\varrho_0) \le v_0$, in which ϱ_0 is the initial state. Equation (44) implies that $V_1(\varrho)$ and ϱ can converge to zero within finite time. Meanwhile, (45) indicates that $V_1(\varrho)$ and ϱ can converge to zero after $t = 2V_1^{0.5}(\varrho_0)\varepsilon^{-1}$ unit of time. If the control gains k_1, k_2 and λ_2 meet the conditions mentioned in (27), the sliding surface $s = \dot{e} + \lambda e$ also converges to zero in finite time. Thus, it can be concluded that the lateral tracking error can achieve asymptotic convergence, that

$$\lim_{t\to\infty} e = 0\,, \text{ and } \lim_{t\to\infty}\dot{e} = 0\,. \tag{46}$$

The above steps complete *Proposition 2* and *Remark.*

IV. SIMULATION RESULTS AND ANALYSIS

To avoid accidents in road tests, simulation tests are carried out to evaluate the performance of the proposed controller. It is noted that the conventional SMC without considering system perturbations is given by (19) and (20). The vehicle parameters are given in Table I. The controller parameter for *Stanely* controller is set as $k = 9$, while for conventional SMC, the controller parameters are set to $\lambda = 9$ and $\alpha_1 = 4.5$. The control input for the proposed STA with considering system perturbations is given by (27). It can be regarded as a nonlinear PID control law with dynamic state feedback. The gains for this controller are set as $\lambda = 9$, $k_1 = 4.5$, $k_2 = 5$, $\lambda_1 = 1.2$, $\lambda_2 = 1.2$, and $\xi^+ = 5$. The related vehicle parameters can be found in Table I. The details of performance evaluation are introduced in the following sub-sections. Given that the sideslip angle is hard to acquire by vehicle onboard sensors, a sliding mode observer mentioned in [44] is used for observing the sideslip angle.

The validation platform is implemented based on the commercial software, Matlab/Simulink and Carsim. The Carsim software provides a full vehicle model, which can describe the coupled vehicle dynamic performance and behavior sophisticatedly.

A. NOVEL EVALUATION INDEX FOR CONTROLLER PERFORMANCE

As the path following control is highly related to vehicle lateral dynamics, the proposed evaluation index consists of yaw rate error $e_{yawrate} = \dot{\varphi} - \dot{\varphi}_{ref}$, control input front-steering angle, and lateral tracking error $e_{trc} = Y_{real} - Y_{ref}$,

This article has been accepted for publication in a future issue of this journal, but has not been fully edited. Content may change prior to final publication. Citation information: DOI 10.1109/ACCESS.2021.3110435, IEEE Access

where Y_{real}^{i} and Y_{ref}^{i} are the i_{th} coordinates for real lateral tracking point and desired path point in the world coordinate system respectively [45].

1) The integral absolute lateral tracking and yaw rate errors ($IATE$) is:

$$IATE = \int_0^t \left(|e_{trc}| + |e_{yawrate}|\right)dt\,. \tag{47}$$

2) The integral time product of the absolute lateral tracking error and yaw rate error (i.e. $IAPE$) is:

$$IAPE = \int_0^t t\left(|e_{trc}| + |e_{yawrate}|\right)dt\,. \tag{48}$$

3) The integral of the absolute value of the front steering angle (i.e. $IASA$) is:

$$IASA = \int_0^t |\delta_f|dt\,, \tag{49}$$

where t is control time duration.

The $IAPE$ acts as a complement for $IATE$, which does not consider the time duration. To make the above-mentioned indexes more generally and objectively, a dimensionless integrated and weighted performance evaluation index (i.e. $IWPEI$) is defined as

$$\begin{aligned} IWPEI &= \frac{\omega_1}{\max\left(|e_{trc}|, |e_{yawrate}|\right)t} IATE \\ &+ \frac{\omega_2}{\max\left(|e_{trc}|, |e_{yawrate}|\right)t^2} IAPE \\ &+ \frac{\omega_3}{|\delta_f|_{max}\, t} IASA \end{aligned} \tag{50}$$

where ω_1, ω_2 and ω_3 are user-defined weights for the three indexes respectively, and $\omega_1 + \omega_2 + \omega_3 = 1$. The value of $\max\left(|e_{trc}|, |e_{yawrate}|\right)$ can be set according to the experimental results. $|\delta_f|_{max}$ represents the maximum front steering angle. Since the performances quantified by the three indexes are considered equally important with each other in the evaluation, the weights ω_1, ω_2 and ω_3 are set as an equal value of 1/3 in this simulation test. The weights are selected to penalize the lateral tracking error and minimize the control input. The smaller the $IWPEI$, the better the performance.

B. PATH FOLLOWING SIMULATION TEST RESULTS WITH KNOWN PARAMETERS UNDER NORMAL DRIVING

In this normal driving scenario, conservative motion planning received from the upper planning layer is assumed. That is to say, the tires are operated in the linear region. The longitudinal speed profiles also behave in the normal range, which is close to that of the average speed of daily transport. As shown in Figure 5, a variable curvature built-in handling course in Carsim is adopted to test the performance of the controllers. The corresponding curvatures and longitudinal speed profiles for this course are shown in Figure 6. The

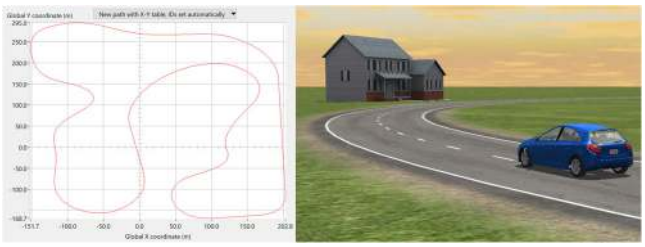

FIGURE. 5. Built-in handling course in Carsim.

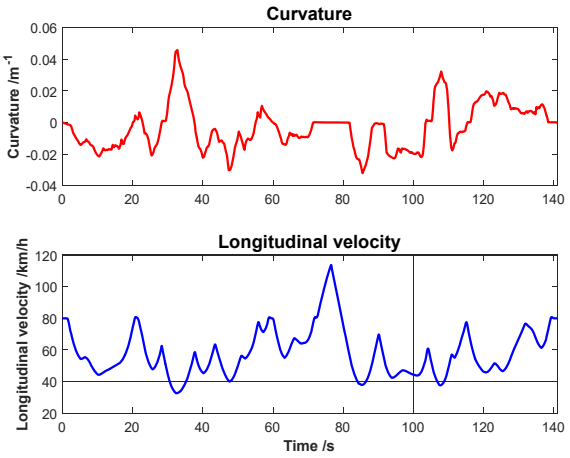

FIGURE. 6. Handling course curvature and longitudinal velocity.

TABLE I
VEHICLE PARAMETERS FOR SINGLE-TRACK MODEL AND SIMULATION

Symbol	Value	Unit
m	1270	kg
μ	0.85	–
C_f	25750	N/rad
C_r	34950	N/rad
l_f	1.015	m
l_r	1.895	m
I_z	1536.7	kg·m^2

TABLE II
TIRE PARAMETERS

Symbol	Value	Unit
--	Tire A	215/55/R17
--	Tire B	185/65/R15
C_f, C_r	Cornering stiffness at $F_{z,Norm}$ (Tire A)	27525/N/rad
C_f, C_r	Cornering stiffness at $F_{z,Norm}$ (Tire B)	33750/N/rad
$F_{z,Norm}$	Nominal vertical force	5500/N
$F_{y,max}$	Maximum lateral force at $F_{z,Norm}$ (Tire A)	5100/N
$F_{y,max}$	Maximum lateral force at $F_{z,Norm}$ (Tire B)	5400/N

curvature ranges from -0.032m^{-1} to 0.0458m^{-1}. The longitudinal velocity V_x varies between 32.5km/h and

This article has been accepted for publication in a future issue of this journal, but has not been fully edited. Content may change prior to final publication. Citation information: DOI 10.1109/ACCESS.2021.3110435, IEEE Access

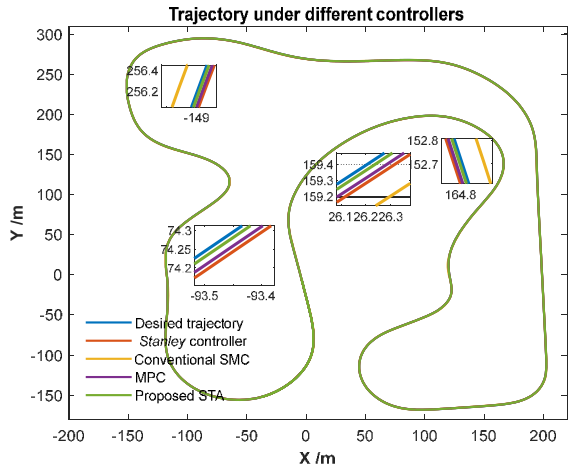

FIGURE. 7. Trajectory comparison under different controllers for normal driving.

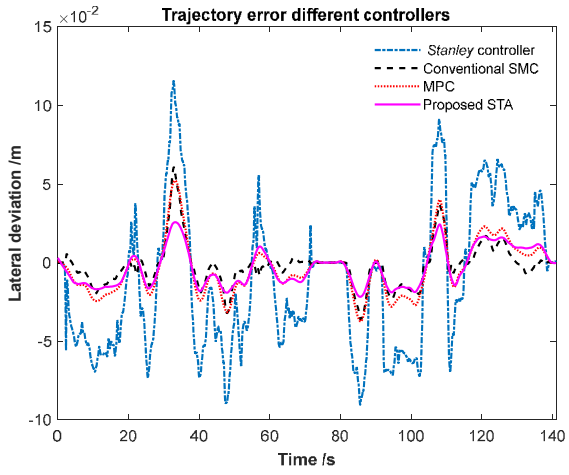

FIGURE. 8. Lateral deviation with respect to desired path for normal driving.

TABLE III
EVALUATION INDEX AND COMPUTATION TIME COMPARISON IN NORMAL DRIVING SCENARIO

Index	*Stanley* controller	Conventional SMC	MPC	Proposed STA
IWPEI	87.1%	72.4%	57.5%	46.6%
Computation time	70.2ms	93.6ms	337ms	95ms

113.6km/h. The simulation results are shown in Figure 7 to Figure 10 with the known nominal vehicle mass and the same tire parameters. It is noted that the path length of the built-in handling course in Carsim is 2273.848m, which requires a long travelling time of about 141 seconds to finish as shown in the x-axis of Figure 8 to Figure 10.

Figure 7 presents that both the benchmark controllers and proposed STA controller can maintain the vehicle driving along the desired trajectory. Their lateral deviations with respect to the desired path are small, in which the maximum value is less than 0.12m as shown in Figure 8. Compared

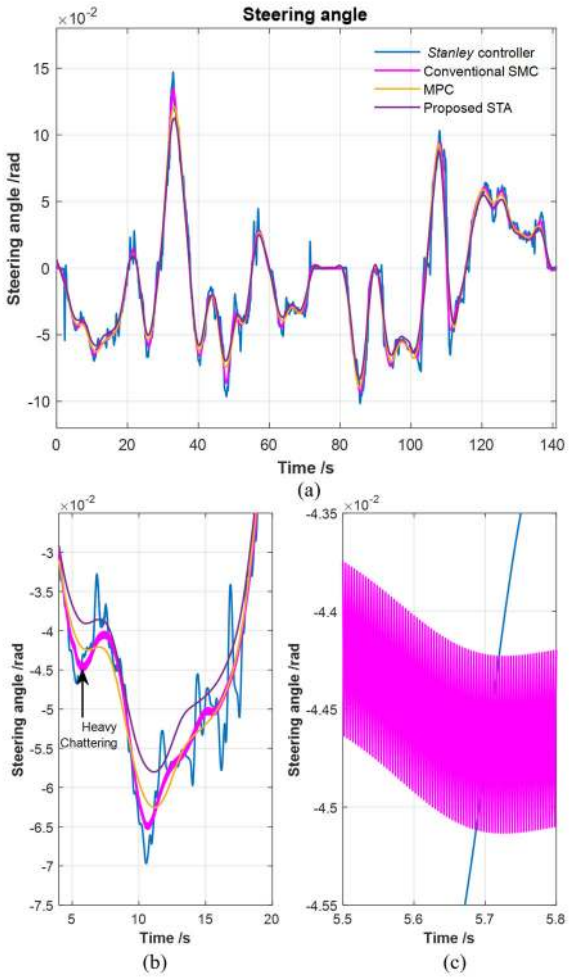

FIGURE. 9. Steering angles with enlarged details under different controllers for normal driving.

with other benchmark controllers, the proposed STA can effectively restrain the lateral deviation even in tight turns.

Figure 9 gives the control inputs of the front steering wheel angles of both controllers. Compared with the benchmark controllers, the proposed STA gives a continuous and smooth control input without chattering and sharp changes. The control effort behaves smaller than the *Stanley* controller, conventional SMC, and MPC.

Figure 10 depicts that the yaw rate performance is also better than other benchmark controllers with the smoother variation under a large change of steering angle. Table III shows that the *IWPEI* of the proposed STA is reduced by 40.5%, 25.8%, and 10.9%, respectively, as compared with the three benchmark controllers in the normal case (Tire A and $m = 1270$ kg).

In addition, the computer in the simulation equips with an Intel(R) Core(TM) i7-4600U CPU and 8.00 GB RAM. As shown in Table III, the computation time of the MPC controller is nearly 337 milliseconds, which is slower than *Stanley* controller, conventional SMC and the proposed STA

This article has been accepted for publication in a future issue of this journal, but has not been fully edited. Content may change prior to final publication. Citation information: DOI 10.1109/ACCESS.2021.3110435, IEEE Access

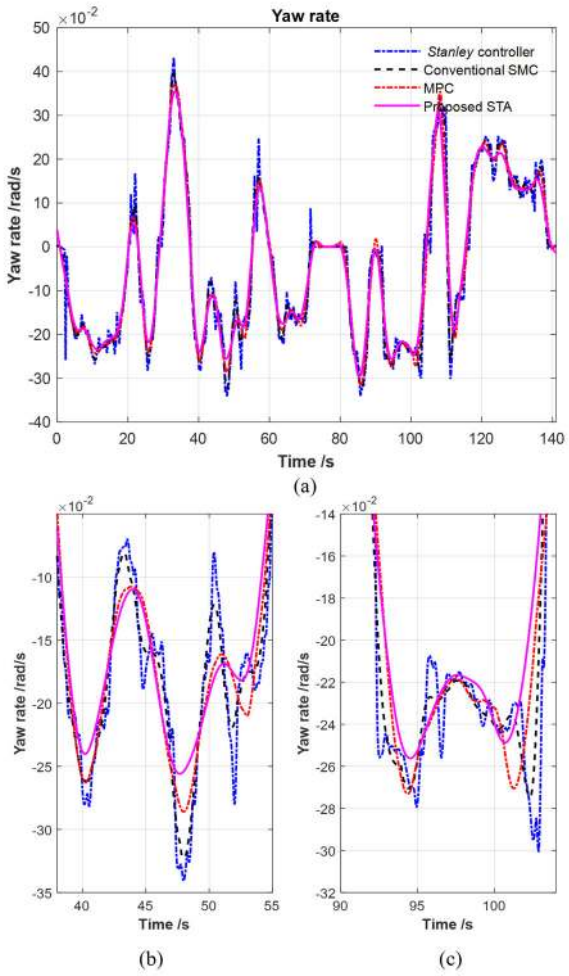

FIGURE. 10. Yaw rates under different controllers for normal driving.

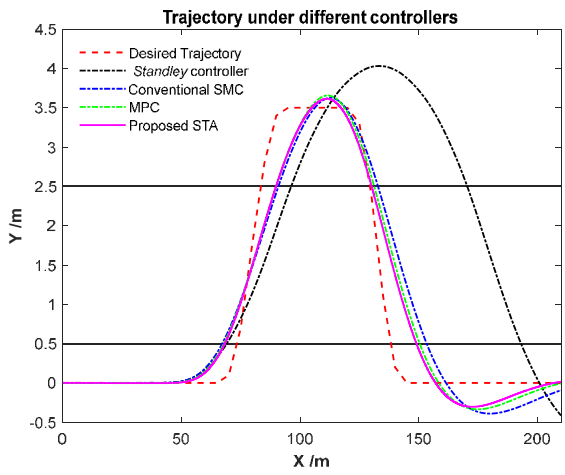

FIGURE. 11. Trajectory comparison under different controllers in DLC scenario.

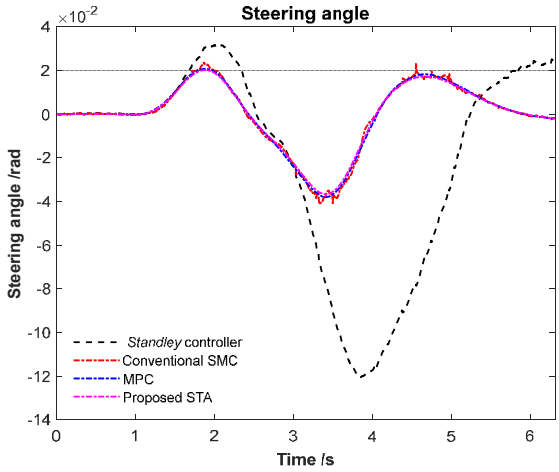

FIGURE. 12. Steering angles under different controllers in DLC scenario.

by 4.8 times, 3.6 times, and 3.55 times, respectively. The reason is that the *Stanley* controller is the simplest one among the four types of control methods. However, its overall control performance is not so good compared with the other three controllers. Comparing *Stanley* controller and the MPC, the proposed STA gives a very good balance between the control performance and the computational cost.

C. DOUBLE LANE CHANGE SCENARIO

To evaluate the controller performance under the fierce driving mode, a double lane change (DLC) scenario recommended by ISO 3888:1 2018 is adopted here. In this scenario, the longitudinal velocity is set as $V_x = 120$ km/h. Simulation results are given in Figure 11 to Figure 14.

As shown in Figure 11, the *Standley* controller cannot react quickly enough to follow the desired trajectory. The conventional SMC, MPC, and the proposed STA controllers present a good trajectory tracking performance under a high longitudinal velocity in the DLC scenario. The simulation results of conventional SMC present a chattering phenomenon as shown in Figure 12 to Figure 14. As presented in Table IV,

TABLE IV
EVALUATION INDEX AND COMPUTATIONAL TIME COMPARISON IN DLC SCENARIO

Index	*Stanley* controller	Conventional SMC	MPC	Proposed STA
IWPEI	80.8%	42.3%	25.1%	18.3%
Computation time	76ms	94ms	314ms	96ms

the proposed STA performs the best with the smallest $IWPEI = 18.3\%$, followed by $IWPEI = 25.1\%$ for MPC, $IWPEI = 42.3\%$ for conventional SMC, and $IWPEI = 80.8\%$ for *Standley* controller. Therefore, the proposed STA controller has a better control performance compared with the other benchmark controllers.

In the DLC scenario, the MPC still needs more computation time compared to the other three controllers. Table IV depicts that the MPC takes about 314 milliseconds for computation, which is slower than *Stanley* controller, conventional SMC

This article has been accepted for publication in a future issue of this journal, but has not been fully edited. Content may change prior to final publication. Citation information: DOI 10.1109/ACCESS.2021.3110435, IEEE Access

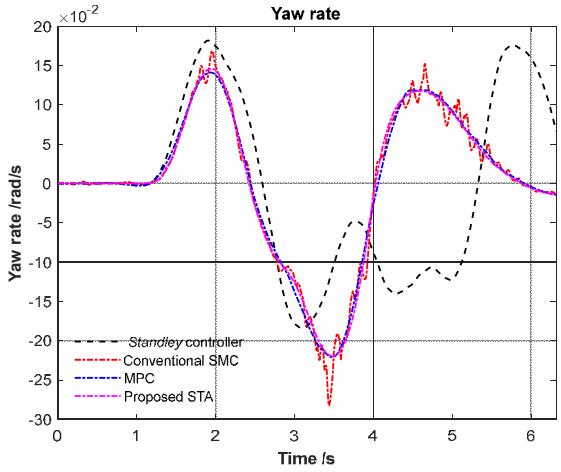

FIGURE. 13. Yaw rates under different controllers in DLC scenario.

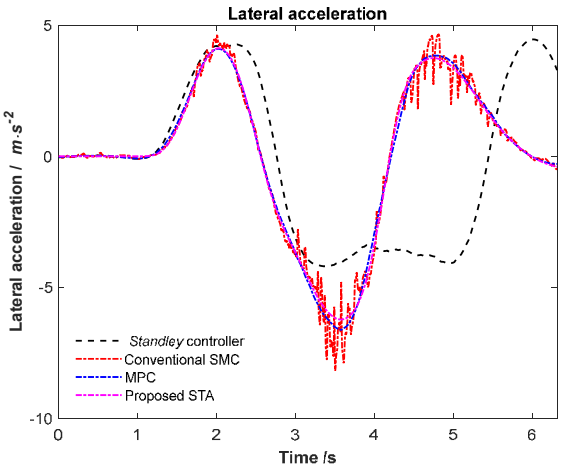

FIGURE. 14. Larger accelerations under different controllers in DLC scenario.

and the proposed STA by 4.1 times, 3.3 times, and 3.27 times, respectively. Given the good control performance and acceptable computation time, the proposed STA is more suitable for real-time path following control of autonomous vehicles.

D. ROBUSTNESS VERIFICATION FOR PROPOSED CONTROLLER

For the path following controller, the other major challenge is the robustness against vehicle model uncertainties, perturbations, and driving condition change.

This subsection demonstrates the robustness under a time-varying vehicle mass and two different tires. The simulation test is conducted at the co-simulation platform. Different tire parameters are described in Table II. Generally, it is difficult to accurately estimate the cornering stiffness because it considerably varies with vertical load, road conditions, and suspension parameters, etc. In addition, the vehicle mass also affects controller performance significantly. The mass is also

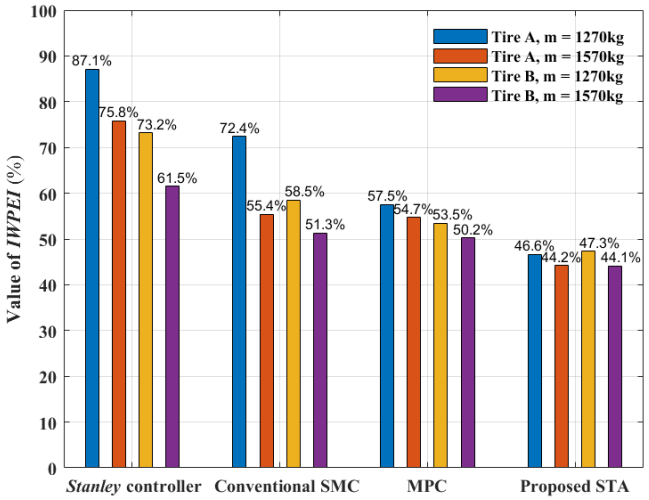

FIGURE. 15. *IWPEI* in robustness test for different controllers.

TABLE V
FLUCTUATION OF *IWPEI* UNDER DIFFERENT CONTROLLERS

Index	*Stanley* controller	Conventional SMC	MPC	Proposed STA
$Per_{Controller}$	29.4%	29.1%	12.7%	6.8%

hard to estimate because of the varying number of persons in the car, weight of fuel, etc. Therefore, it is important to verify the robustness of the proposed controller.

The controller performance evaluation index *IWPEI* is illustrated in Figure 15. By changing the vehicle mass and tire simultaneously, the fluctuation of the *IWPEI* can be calculated by using the percentage of *IWPEI* change:

$$Per_{\text{Controller}} = \left| \frac{\max(IWPEI) - min(IWPEI)}{\max(IWPEI)} \right|. \quad (51)$$

Table V shows that $Per_{\text{Proposed STA}}$ is less than $Per_{Stanley}$, $Per_{\text{Conventional SMC}}$, and Per_{MPC} by 22.6%, 22.3%, and 5.9%, respectively. Therefore, the proposed STA is insensitive to vehicle weight change and tire parameter variation. It should be emphasized that the proposed STA always gives a minimum $Per_{\text{Controller}}$ value regardless of varying vehicle mass and tire parameters, and produces small, continuous, and smooth control input compared with the benchmark controllers.

In a word, the proposed STA exhibits better performance than *Stanley* controller, conventional SMC, and MPC according to the simulation results and overall performance analysis.

V. CONCLUSION

In this work, a novel super-twisting sliding mode controller is designed with considering perturbations for autonomous vehicle path following problem. The control performance is evaluated based on a novel *IWPEI* proposed in this work, which consists of control input, lateral deviation, and yaw rate error. Comparing the benchmark *Stanley* controller,

conventional SMC, and MPC, the simulation results show that the proposed STA generates a continuous control input without chattering problem, resulting in a smaller lateral deviation and smoother yaw rate. Besides, the robustness of the controller is tested with the varying vehicle mass and tire parameters under the same controller parameters. Simulation results also show that the robustness of the proposed STA outperforms the benchmark controllers with the smallest $Per_{\text{Controller}}$. In summary, the overall performance of the proposed STA is better than the benchmark controllers because of the smooth front steering angle and yaw rate without chattering and small lateral error.

Future work will consider the learning-based path following controller design. Moreover, the hardware and real vehicle experiments will be considered in the upcoming path following research.

REFERENCES

[1] S. Thrun, M. Montemerlo, H. Dahlkamp, D. Stavens, A. Aron, J. Diebel, …, and K. Lau, "Stanley: The robot that won the DARPA Grand Challenge," *Journal of Field Robotics,* vol. 23, no. 9, pp. 661-692, 2006.

[2] J. Ni, J. Hu, and C. Xiang, "Robust path following control at driving/handling limits of an autonomous electric racecar," *IEEE Transactions on Vehicular Technology,* vol. 68, no. 6, pp. 5518-5526, 2019.

[3] Y. Wang, C. Zong, H. Guo, and H. Chen, "Fault tolerant path following control for in-wheel-motor-driven autonomous ground vehicles with differential steering," *Asian Journal of Control,* vol. 22, no. 3, pp. 1230-1240, 2020.

[4] C. Hu, R. Wang, and F. Yan, "Integral sliding mode-based composite nonlinear feedback control for path following of four-wheel independently actuated autonomous vehicles," *IEEE Transactions on Transportation Electrification,* vol. 2, no. 2, pp. 221-230, 2016.

[5] Y. Wu, L. Wang, J. Zhang, and F. Li, "Path following control of autonomous ground vehicle based on nonsingular terminal sliding mode and active disturbance rejection control," *IEEE Transactions on Vehicular Technology,* vol. 68, no. 7, pp. 6379-6390, 2019.

[6] R. Wang, H. Jing, C. Hu, F. Yan, and N. Chen, "Robust H∞ Path Following Control for Autonomous Ground Vehicles With Delay and Data Dropout," *IEEE Transactions on Intelligent Transportation Systems,* vol. 17, no. 7, pp. 2042-2050, 2016.

[7] W. Huang, P. K. Wong, K. I. Wong, C. M. Vong, and J. Zhao, Adaptive neural control of vehicle yaw stability with active front steering using an improved random projection neural network. Vehicle system dynamics, vol. 59, no. 3, pp. 396-414, 2021.

[8] W. Li, Z. Xie, J. Zhao, and P. K. Wong, "Velocity-based robust fault tolerant automatic steering control of autonomous ground vehicles via adaptive event triggered network communication," *Mechanical Systems Signal Processing,* vol. 143, p. 106798, 2020.

[9] J. Zhang, H. Wang, M. Ma, M. Yu, A. Yazdani, and L. Chen, "Active front steering-based electronic stability control for steer-by-wire vehicles via terminal sliding mode and extreme learning machine," *IEEE Transactions on Vehicular Technology,* 2020, DOI: 10.1109/TVT.2020.3036400.

[10] A.-T. Nguyen, C. Sentouh, H. Zhang, and J.-C. Popieul, "Fuzzy static output feedback control for path following of autonomous vehicles with transient performance improvements," *IEEE Transactions on Intelligent Transportation Systems,* vol. 21, no. 7, pp. 3069-3079, 2019.

[11] J. Guo, Y. Luo, and K. Li, "Robust gain-scheduling automatic steering control of unmanned ground vehicles under velocity-varying motion," *Vehicle System Dynamics,* vol. 57, no. 4, pp. 595-616, 2019.

[12] B. Paden, M. Čáp, S. Z. Yong, D. Yershov, and E. Frazzoli, "A survey of motion planning and control techniques for self-driving urban vehicles," *IEEE Transactions on intelligent vehicles,* vol. 1, no. 1, pp. 33-55, 2016.

[13] H. Wang, F. Zhou, Q. Li, and W. Song, "Reliable Adaptive H∞ Path Following Control for Autonomous Ground Vehicles in Finite Frequency Domain," *Journal of the Franklin Institute,* 2020, DOI: 10.1016/j.jfranklin.2020.07.028.

[14] H. Wang and L. Guvenc, "Discrete-time Robust PD Controlled System with DOB/CDOB Compensation for High Speed Autonomous Vehicle Path Following," *SAE Technical Paper*, no. 2019-01-0674, 2019.

[15] Y. Wang, H. Ding, J. Yuan, and H. Chen, "Output-feedback triple-step coordinated control for path following of autonomous ground vehicles," *Asian Journal of Control,* vol. 116, pp. 146-159, 2019.

[16] J. Chen, Z. Shuai, H. Zhang and W. Zhao, "Path Following Control of Autonomous Four-Wheel-Independent-Drive Electric Vehicles Via Second-Order Sliding Mode and Nonlinear Disturbance Observer Techniques," *IEEE Transactions on Industrial Electronics*, 2020, DOI: 10.1109/TIE.2020.2973879.

[17] Z. Chu, Y. Sun, C. Wu, and N. Sepehri, "Active disturbance rejection control applied to automated steering for lane keeping in autonomous vehicles," *Control Engineering Practice,* vol. 74, pp. 13-21, 2018.

[18] Y. Liang, Y. Li, A. Khajepour, and L. Zheng, "Multi-model adaptive predictive control for path following of autonomous vehicles," *IET Intelligent Transport Systems*. 2021, DOI: 10.1049/iet-its.2020.0357.

[19] Y. Wang, C. Zong, H. Guo, and H. Chen, "Fault-tolerant path-following control for in-wheel-motor-driven autonomous ground vehicles with differential steering," *Asian Journal of Control*, vol. 22, no. 3, pp. 1230-1240, 2020.

[20] F. Lin, S. Wang, Y. Zhao, and Y. Cai, "Research on autonomous vehicle path tracking control considering roll stability," *Proceedings of the Institution of Mechanical Engineers, Part D: Journal of Automobile Engineering,* 2020, DOI: 10.1177/0954407020942006.

[21] J. Guo, J. Wang, P. Hu, and L. Li, "Robust guaranteed-cost path-following control for autonomous vehicles on unstructured roads," *Proceedings of the Institution of Mechanical Engineers, Part D: Journal of Automobile Engineering,* vol. 232, no. 7, pp. 896-908, 2018.

[22] A.-T. Nguyen, C. Sentouh, and J.-C. Popieul, "Fuzzy steering control for autonomous vehicles under actuator saturation: Design and experiments," *Journal of the Franklin Institute,* vol. 355, no. 18, pp. 9374-9395, 2018.

[23] X. Ji, X. He, C. Lv, Y. Liu, and J. Wu, "Adaptive-neural-network-based robust lateral motion control for autonomous vehicle at driving limits," *Control Engineering Practice,* vol. 76, pp. 41-53, 2018.

[24] Z. Tang, X. Xu, F. Wang, X. Jiang, and H. Jiang, "Coordinated control for path following of two-wheel independently actuated autonomous ground vehicle," *IET Intelligent Transport Systems,* vol. 13, no. 4, pp. 628-635, 2018.

[25] J. Ghommam, S. E. Ferik, and M. Saad, "Robust adaptive path-following control of underactuated marine vessel with off-track error constraint," *International Journal of Systems Science,* vol. 49, No. 7, pp. 1540-1558, 2018.

[26] Z. Peng, J. Wang, and Q.-L. Han, "Path-following control of autonomous underwater vehicles subject to velocity and input constraints via neurodynamic optimization," vol. 66, no. 11, pp. 8724-8732, 2018.

[27] K. Lee, S. E. Li, and D. Kum, "Synthesis of robust lane keeping systems: impact of controller and design parameters on system performance," *IEEE Transactions on Intelligent Transportation Systems,* vol. 20, no. 8, pp. 3129-3141, 2018.

[28] X. Du, K. K. K. Htet, and K. K. Tan, "Development of a genetic-algorithm-based nonlinear model predictive control scheme on velocity and steering of autonomous vehicles," *IEEE Transactions on Industrial Electronics,* vol. 63, no. 11, pp. 6970-6977, 2016.

[29] S. Gong, J. Shen, and L. Du, "Constrained optimization and distributed computation based car following control of a connected and autonomous vehicle platoon," *Transportation Research Part B: Methodological,* vol. 94, pp. 314-334, 2016.

[30] J. Guo, Y. Luo, and K. Li, "An adaptive hierarchical trajectory following control approach of autonomous four-wheel independent drive electric vehicles," *IEEE Transactions on Intelligent Transportation Systems,* vol. 19, no. 8, pp. 2482-2492, 2017.

[31] R. Rout and B. Subudhi, "Inverse optimal self-tuning PID control design for an autonomous underwater vehicle," *International Journal of Systems Science,* vol. 48, no. 2, pp. 367-375, 2017.
[32] P. Hang, X. Chen, and F. Luo, "LPV/H∞ controller design for path tracking of autonomous ground vehicles through four-wheel steering and direct yaw-moment control," *International Journal of Automotive Technology*, vol. 20, no. 4, pp. 679-691, 2019.
[33] G. Tagne, R. Talj, and A. Charara, "Design and comparison of robust nonlinear controllers for the lateral dynamics of intelligent vehicles," *IEEE Transactions on Intelligent Transportation Systems,* vol. 17, no. 3, pp. 796-809, 2015.
[34] G. Tagne, R. Talj, and A. Charara, "Design and validation of a robust immersion and invariance controller for the lateral dynamics of intelligent vehicles," *Control Engineering Practice,* vol. 40, pp. 81-92, 2015.
[35] R. Wang, C. Hu, F. Yan, and M. Chadli, "Composite nonlinear feedback control for path following of four-wheel independently actuated autonomous ground vehicles," *IEEE Transactions on Intelligent Transportation Systems,* vol. 17, no. 7, pp. 2063-2074, 2016.
[36] H. Guo, D. Cao, H. Chen, Z. Sun, and Y. Hu, "Model predictive path following control for autonomous cars considering a measurable disturbance: Implementation, testing, and verification," *Mechanical Systems and Signal Processing,* vol. 118, pp. 41-60, 2019.
[37] C. Yin, B. Xu, X. Chen, Z. Qin, Y. Bian, and N. Sun, "Nonlinear Model Predictive Control for Path Tracking Using Discrete Previewed Points," 2020 IEEE 23rd International Conference on Intelligent Transportation Systems (ITSC), 2020, pp. 1-6
[38] Z. Lin, J. Duan, S. E. Li, H. Ma, Y. Yin, and B. Cheng, "Continuous-time finite-horizon ADP for automated vehicle controller design with high efficiency," 2020 3rd International Conference on Unmanned Systems (ICUS), 2020, pp. 978-984.
[39] T. Chen, L. Chen, X. Xu, Y. Cai, H. Jiang, and X. Sun, "Passive fault-tolerant path following control of autonomous distributed drive electric vehicle considering steering system fault," *Mechanical Systems and Signal Processing,* vol. 123, pp. 298-315, 2019.
[40] G. Tagne, R. Talj, and A. Charara, "Higher-order sliding mode control for lateral dynamics of autonomous vehicles, with experimental validation," in *2013 IEEE Intelligent Vehicles Symposium (IV)*, 2013, pp. 678-683: IEEE.
[41] J. A. Moreno and M. Osorio, "A Lyapunov approach to second-order sliding mode controllers and observers," in *2008 47th IEEE conference on decision and control*, 2008, pp. 2856-2861: IEEE.
[42] F. Muñoz, M. Bonilla, I. González-Hernández, S. Salazar and R. Lozano, "Super Twisting vs Modified Super Twisting algorithm for altitude control of an Unmanned Aircraft System," 2015 12th International Conference on Electrical Engineering, Computing Science and Automatic Control (CCE), 2015, pp. 1-6.
[43] H. K. Khalil and J. W. Grizzle, *Nonlinear systems*. Prentice Hall, NJ, 2002.
[44] S. Ding, L. Liu, and W. X. Zheng, "Sliding mode direct yaw-moment control design for in-wheel electric vehicles," *IEEE Transactions on Industrial Electronics,* vol. 64, no. 8, pp. 6752-6762, 2017.
[45] L. Zhang, H. T. Ding, J. P. Shi, Y. J. Huang, H. Chen, K. H. Guo, and Q. Li, "An Adaptive Backstepping Sliding Mode Controller to Improve Vehicle Maneuverability and Stability via Torque Vectoring Control," *IEEE Transactions on Vehicular Technology,* vol. 69, no. 3, pp. 2598-2612, 2020.